Thermomechanical Degradation of Thermal Interface Materials: Accelerated Test Development and Reliability Analysis

Hayden Carlton
Department of Mechanical Engineering,
University of Arkansas,
700 Research Center Boulevard,
Fayetteville, AR 72701
e-mail: hscarlto@email.uark.edu

Dustin Pense
Department of Mechanical Engineering,
University of Arkansas,
863 W. Dickson Street,
Fayetteville, AR 72701
e-mail: dpense@email.uark.edu

David Huitink[1]
Department of Mechanical Engineering,
University of Arkansas,
863 W. Dickson Street,
Fayetteville, AR 72701
e-mail: dhuitin@uark.edu

Due to the inherently low adhesive strength and structural integrity of polymer thermal interface materials (TIMs), they present a likely point of failure when succumbed to thermomechanical stresses in electronics packaging. Herein, we present a methodology to quantify TIM degradation through an accelerated and repeatable mechanical cycling technique. The testing apparatus incorporated a steady-state thermal conductivity measurement system, consistent with ASTM 5470-06, with added displacement actuation and force sensing to provide controlled cyclic loading between −20 N and 20 N. Additionally, a novel optical technique was utilized to observe void formation, pump-out, and dry-out behavior during cycling, in order to correlate the thermal performance with physical behaviors of different TIMs under cyclic stress. Of the two different pastes analyzed, cyclic testing was found to degrade the thermal performance of the less viscous TIM by increasing its interfacial resistance. Optical qualitative measurements revealed the breakdown of the TIM structure at the interface, which indicated the formation of voids due to TIM degradation. Applying this testing method for future TIM development could help in optimizing TIM structure for particular package applications.
[DOI: 10.1115/1.4047099]

Introduction

A thermal interface material (TIM) refers to a substance that is applied at the interface of two separate surfaces in order to improve the thermal conductivity between them [1]. In the realm of electronic devices, TIMs are often applied at the contact between a device and heat spreader; TIMs at this interface allow for enhanced thermal dissipation, which in turn results in enhanced device operation, as well as improved reliability [2]. Common materials used for TIMs include, but are not limited to, thermal pastes (filler materials) [3], low-melting point metals [4], and carbon-based materials, which utilize the high thermal conductivity of pure carbon [5]. Thermal pastes or greases are arguably the most widely used due to their reasonable performance, low cost, and simple application [1]; thermal pastes are incorporated into everything from industrial-grade power electronics to home computers.

While thermal pastes remain widely used, the main cause for concern has been their reliability when integrated into electronics packaging [3], and research regarding their degradation during normal operation is infrequent. As a device undergoes power cycling throughout typical on/off cycles, mismatch between the coefficient of thermal expansion (CTE) of the device and substrate induces warpage. While this occurrence can prove damaging to the solder joints, CTE mismatch-induced strain also drives shear and peeling stresses at the device/TIM interface; as a result, subsequent on/off cycles can gradually cause thermal pastes to be squeezed out between the device and its heat sink, which is intuitively referred to as TIM "pump-out" [2]. Another failure mechanism for TIMs occurs at higher temperatures when the filler material is separated from the paste matrix; this occurrence is known as TIM "dry-out." [6]. Both failure mechanisms can negatively affect both the reliability of the TIM at a particular interface as well as reduce its thermal conductivity.

Previous methods in the literature have investigated the thermal performance and reliability of TIMs through various experimental methodologies. Among the more popular ways to characterize TIM thermal conductivity is through steady-state thermal methods, which have been utilized even in recent efforts [7–9]. The popularity of steady-state methods stems from their simplicity, and because of their wide-spread usage, researchers within this field keep improving these methodologies constantly [10,11]. Methods such as these can accurately characterize TIM thermal conductivity in ideal conditions; however, in order to simulate the temperatures that accompany power cycles in real-world applications, other techniques, such as temperature cycling, need to be utilized to determine TIM reliability. In temperature cycling, a paste sample is introduced to an interfacial region, and the environmental temperature is alternated so as to induce CTE-mismatch-driven stresses in the package/assembly. The resulting thermally induced, cyclic stresses induce TIM failure, as often measured through thermal resistance measurements or acoustic imagery of the TIM interfaces. A recent study incorporated acoustic imagery to showcase how TIMs degrade under temperature cycling conditions [12]. Controlled temperature cycling is a well-established process in power electronics, yet a full test can be time-consuming and can often take weeks or months to get a statistically significant result.

Alternatively, mechanical cycling has also shown to be advantageous when testing for failures driven by CTE-mismatch, such as in a recent study by Marbut et al., who developed a rapid reliability test of solder interconnects [13]. Due to the inherently mechanical nature of polymer TIM failure, attempts have been made to use accelerated mechanical cycling to test their reliability [14–16]; instead of varying the temperature to provide stress, mechanical cycling applies force directly to the paste to mimic the strain occuring during temperature cycling, and can offer significantly reduced accelerated testing time. Mechanical cycling provides an avenue through which rapid accelerated tests can be performed to simulate the degradation of thermal pastes during

[1]Corresponding author.

Contributed by the Electronic and Photonic Packaging Division of ASME for publication in the Journal of Electronic Packaging. Manuscript received December 17, 2019; final manuscript received April 1, 2020; published online May 21, 2020. Assoc. Editor: Sukwon Choi.

normal operation. The study within investigates the effects of mechanical cycling on the thermal resistance of TIMs to develop an accelerated reliability test. Accompanying the thermomechanical measurements, a novel method utilizing visual imagery will illustrate the degradation of the TIM structure during testing as well as address possible failure mechanisms.

Materials and Methods

Thermal Testing Apparatus. Thermal resistance was measured using a custom-built thermal conductivity tester that consisted of two cylindrical copper rods, as shown in Fig. 1; this configuration was based on ASTM 5470-06, which describes a standard method for measuring thermal resistance. A 200 W cartridge heater with an integrated thermocouple was embedded at the end of the right copper rod, which provided a heat source and maintained constant temperature via an external proportional-integral-derivative controller. The left copper rod served as a source of heat removal; water at a constant temperature circulated through the center. Eight K-type thermocouples were embedded at regular intervals along each rod (four in each rod) to measure a unidirectional temperature gradient. Each of the rods was surrounded by insulating polyurethane foam and was held in a place by clamps anchored into a wooden base. The alignment and planarity of the copper faces was ensured through the use of blue machining dye. One copper face was coated with the dye and brought into contact with the opposing rod's face; the rods were determined to be aligned when the dye completely coated the face of the opposing rod as a result of the contact.

As displayed in Fig. 1, the heated rod remained stationary and was mounted directly to the wooden base; conversely, the cooled rod was mounted on a sled which was free to move along a linear slide rail. Friction was minimized by utilizing bushings between the sled and rail. A DC servomotor linear actuator adjusted the position of the cooled rod along the linear slide rail. A miniature S-beam load cell connected the actuator to the back of the sliding cooled rod, which measured the tensile and compressive forces exerted on the cooled rod by the actuator. Force and temperature data gathered by the load cell and all eight thermocouples (TC), respectively, were gathered and plotted using a custom-built data acquisition unit.

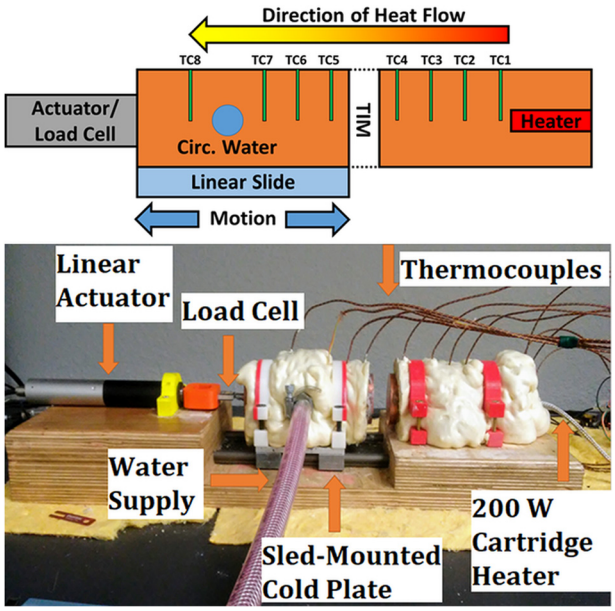

Fig. 1 Diagram of conductivity tester setup and picture of physical test setup

Calculating Thermal Resistance. The testing apparatus utilized Fourier's law of conduction to measure steady-state thermal resistance of the thermal paste; in the unidirectional case, this law simplifies to Eq. (1), where q_x is the heat flux in one dimension, k is the thermal conductivity, and dT/dx is the temperature gradient in the direction of the heat flux

$$q_x\left(\frac{W}{m^2}\right) = -k\frac{dT}{dx} \tag{1}$$

If the law is further simplified to quantify total heat transfer Q in a given area and solved for thermal resistance, the equation becomes Eq. (2), where ΔT is the change in temperature over a given bond line thickness (BLT), and R is the thermal resistance, equivalent to L/kA. In this case, L is the BLT of the TIM at the interface of the two rods, and A is the cross-sectional area

$$R\left(\frac{^\circ C}{W}\right) = \frac{\Delta T}{Q} \tag{2}$$

In accordance with the ASTM 5470-06 standard, calculation of the heat transfer through the thermal paste sample consisted of taking an average, Q_{AVG} (Eq. (5)), of the measured heat transfer through the heated rod, Q_H (Eq. (3)) and the cooled rod, Q_C (Eq. (4)), where k is the conductivity of copper (400 W/m K), T_i is the temperature indicated by thermocouple "i," and d_{ij} is the distance between thermocouples "i" and "j"

$$Q_H(W) = \frac{kA(T_1 - T_4)}{d_{14}} \tag{3}$$

$$Q_c(W) = \frac{kA(T_5 - T_7)}{d_{57}} \tag{4}$$

$$Q_{AVG}(W) = \frac{Q_H + Q_C}{2} \tag{5}$$

In order to accurately calculate the change in temperature across the thermal paste sample, the exact temperature of the heated (T_H) and cooled (T_C) surfaces in contact with the specimen must be known; Fig. 2 diagrams the heat flow through sample area.

Since TC 4 and TC 5 do not give the exact temperature at the surface of their respective rods, the temperatures have to be approximated based on material properties and experimental data. With the distance between thermocouple "i" and the surface of the rod in contact with the paste sample (d_{is}) known, assuming a linear thermal gradient at steady-state, these surface temperatures can be calculated using the following equations:

$$T_H(^\circ C) = T_4 - \frac{|d_{4s}|}{|d_{14}|} * (T_1 - T_4) \tag{6}$$

$$T_C(^\circ C) = T_5 + \frac{|d_{5s}|}{|d_{57}|} * (T_5 - T_7) \tag{7}$$

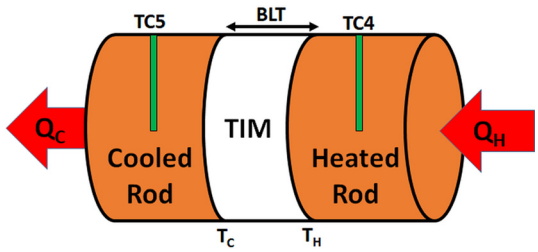

Fig. 2 Heat flow through TIM at the interface between heated and cooled copper rods

With the knowledge of both the change in temperature and heat transfer across the thermal paste specimen, Eq. (2) can be rewritten as Eq. (8), which represents the total thermal resistance of the specimen

$$R\left(\frac{^\circ C}{W}\right) = \frac{T_H - T_C}{Q_{AVG}} \tag{8}$$

This simple measure of thermal resistance at steady-state has been used consistently in the past to study TIM behavior [17], and it has served as the basis for measuring the change in thermal resistance due to thermomechanical degradation of the paste over time. However, accompanying this method's simplicity and wide functionality are some fundamental limitations. When not performed in a perfect vacuum, thermal losses present themselves in the form of convection to the surroundings. Losses such as these can be significantly mitigated with proper insulation (polyurethane foam and wooden base); however, they never completely disappear. Also present during these tests is the small amount of contact resistance between the thermal paste and the surface of the copper rods. Thermal pastes are designed to reduce contact resistances, but they are still present, nevertheless. Since the purpose of these tests is to measure relative change in thermal resistance between periods of mechanical cycling, both contact resistance and losses to the surroundings are assumed negligible.

Visualizing the Interface. When the test apparatus was used to gather visual data, the cooled copper rod was replaced with a three-dimensional printed part which consisted of two acrylic windows joined by four pieces of all-thread and secured with eight lock-nuts, as shown in Fig. 3. A camera was mounted in the open space in the center of the part which permitted the viewing of void formations occurring at the interfacial region between the acrylic and heat copper rod.

For gathering visual data, an initial image taken directly after applying the paste served as the control. Images of the acrylic/copper interface were gathered in regular intervals throughout each test and qualitatively compared against the control. The clear acrylic allowed for the formation of voids within the paste to be visually apparent. In order to emulate the copper rod tests, the temperature setting of the cartridge heater was tuned in order to reach a similar interfacial temperature. Essentially, tests performed with the copper rod setup in Fig. 1 were repeated with the visualization setup in Fig. 3, so that both the thermal resistance and paste structure could be characterized throughout the duration of a typical test.

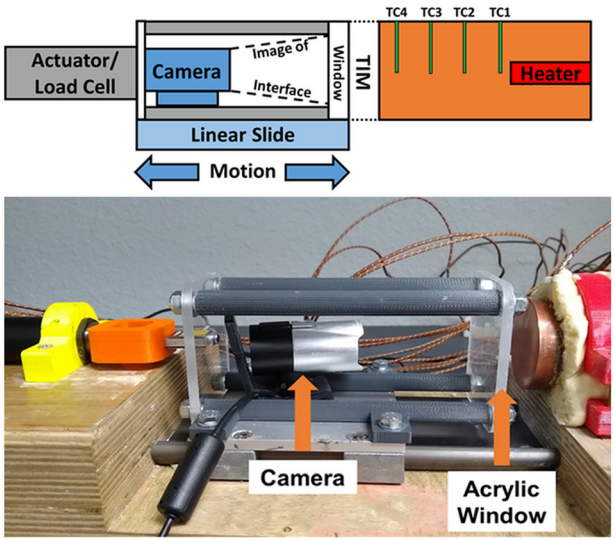

Fig. 3 Diagram and picture of setup to gather visual data

Materials: Thermal Paste. This study investigated two distinct types of commercially available paste. In order to be an encompassing reliability test, this methodology must be capable of analyzing the innumerable different kinds of thermal pastes currently on the market. For this reason, the two pastes chosen differed widely in their material properties and thermal conductivity.

Paste Composition. Table 1 highlights important properties for each of the tested pastes. The most apparent difference between the two paste types, paste 1 and 2, is their matrix material; paste 2 is a viscous nonsilicone-based paste while a less viscous silicone oil-based matrix comprises paste 1. Both pastes contain a significant amount of filler material, zinc and/or aluminum oxide. There also exists a large disparity between their thermal conductivities as well, with paste 2 having a significantly higher thermal conductivity than paste 1; values for thermal conductivity and paste composition were reported by the vendors.

Paste Dynamic Viscosity Measurements. To determine how the dynamic viscosity of the two pastes changed with respect to shear rate, each paste was analyzed using a Rheosys Merlin VR Rheometer (Princeton, NJ). Each paste underwent constant temperature rheological testing at 80 °C using parallel plates with a gap of 1 mm. The shear rate linearly increased from 1 to 120 s^{-1}, and the viscosity was extracted by analyzing the torque exerted on the plates.

Thermal Interface Material Application. Before each TIM application, the faces of the hot and cold rods were polished and cleaned with acetone in order to remove copper oxidation. After turning on the heater/circulating water and allowing each rod to reach steady-state temperature, the linear actuator pressed two rods together with a force of 20 N. The position of the actuator was noted and served as a baseline to measure the BLT of the paste. To ensure that the layer of TIM was uniform and the same mass of paste was used consistently, a tool was created, as shown in left panel in Fig. 4, which consisted of a blue ring that attached to the surface of the heated copper rod. The tool creates a "pocket" on the face of the heated rod, which is filled with TIM; a putty knife was used to remove any excess TIM. After the TIM was applied and smoothed, the tool was removed, revealing the prepared sample at a constant thickness. The application of a consistent layer of thermal paste was necessary to ensure ideal contact and heat transfer between the two copper rods. Upon removal of the tool, the actuator compressed the TIM sample between the two copper rods at a force of 20 N; the difference in position between this point and the baseline, as indicated by the linear actuator was recorded as the paste's BLT. As a control, the BLT of each test was maintained within the range of 4–8 mil.

Static Testing. Once the TIM was successfully applied and allowed to reach steady-state at 80 °C, the sample endured isothermal static testing using the visualization apparatus, where the paste was compressed over a 36-h period. The force on the sample was kept constant at 20 N in compression for the duration of the static test, and the paste structure was observed over time. This test illustrated the degradation of the paste from simply thermal mechanisms, without the influence of mechanical cycling.

Cyclic Testing. During cyclic testing, the TIM sample underwent mechanical cyclic loading provided by the linear actuator. Cyclic loading allowed for observation of the effect of both thermal and mechanical degradation and was compared to the static test results. One cycle consisted of straining the paste to a set percentage of its BLT (placing the paste under tension) and returning to its nominal position (compressing the paste). This type of testing was grouped into periods of 100 cycles, at 0.5 cycles/s. An initial steady-state resistance measurement provided a starting point before the first period of cycles began. Immediately following each period, the TIM sample was allowed to return to steady-state

Table 1 Properties of the thermal pastes tested

	Paste 1	Paste 2
Matrix material	Silicone oil	Nonsilicone oil
Filler material	Zinc oxide (50–80 wt %)	Zinc oxide (10–25 wt %) Aluminum oxide (60–80 wt %)
Viscosity at 80 °C (Pa·s)	198	745
Thermal conductivity (W/m K)	0.75	3.3

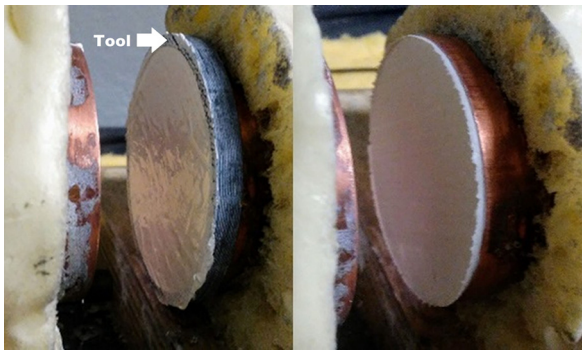

Fig. 4 (Left) Tool used to apply the paste; (right) removal of the tool leaves uniform layer of paste on the surface of the copper rod

temperature, and a resistance measurement was recorded. Each paste underwent three separate cyclic loading conditions, 15%, 20%, and 30% strain, at two different temperatures, 50 °C and 80 °C. An increase in resistance in the context of these trials correlates with thermomechanical degradation of the paste at the interface of the two copper rods. This type degradation presents itself mainly through the occurrence of TIM pump-out, which is compounded by the accelerated mechanical cycling test at increased temperatures. The test gradually increases thermal resistance at the interface of the two rods through the removal of paste from the interface, as well as from the formation of air pockets, which is detrimental to the paste's functionality.

Results and Discussion

Thermal Paste Viscosity. The change in the viscosity of each paste at 80 °C with respect to shear rate is represented in Fig. 5; the initial measured viscosity for both pastes is shown in Table 1. Both pastes exhibited rapid shear thinning behavior, as indicated by the exponential decay in viscosity with respect to increasing shear rate. As portrayed in Table 1, paste 2 has significantly higher viscosity at lower shear rates than paste 1. Also for paste 2, the viscosity data begin to display larger margins of error after 80 s^{-1}; due to the nature of the parallel plate rheometer test, viscosity is determined as a function of the torque exerted on the rotating plate by the sample, which is dependent on the area of contact of the paste between the two plates. As the viscosity of the paste decreases, it gradually spreads out between the two plates, which can give erroneous viscosity measurements at high enough shear rates.

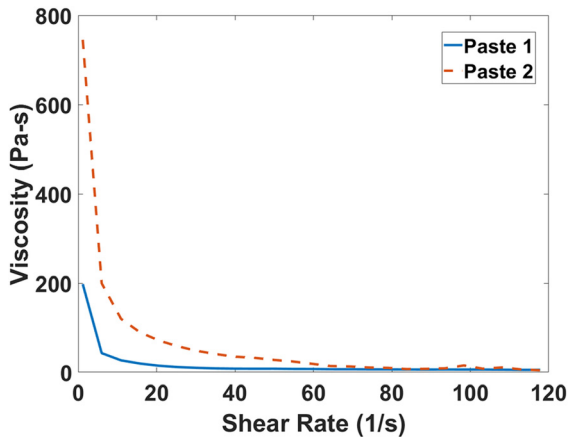

Fig. 5 Dynamic viscosity with respect to shear rate for both pastes at 80 °C

Static Test Results. During the 36 h test where both paste samples underwent a compressive, static load at 80 °C, visual data were gathered using the setup shown in Fig. 3; images taken before and after static testing for both pastes can be seen in in Fig. 6. The top row of Fig. 6 represents paste 1 before (1-1) and after (1-2) static testing, while the bottom row shows paste 2 before (2-1) and after (2-2) static testing.

The visual transition of the paste 1 before and after static testing was found to be quite dramatic; while the pristine paste 1 had virtually no void formation (1-1), the image taken after the 36 h static test (1-2) displayed an interface ridden with voids and areas with inhomogeneities. Since no cyclic testing was performed, it can be inferred that the method of paste degradation is not necessarily TIM pump-out. Possible explanations are the onset of TIM dry-out (the separation of the silicone matrix from the filler material) or even the coalescence of voids introduced during the past application process. Both explanations could be exacerbated by increased temperature at the interface for a prolonged period of time.

As opposed to paste 1, which exhibited a drastic transition over the 36-h test period, paste 2 observed no noticeable void formation or degradation (2-1 and 2-2). Resistance to paste failure most likely stems from its material properties, such as higher viscosity

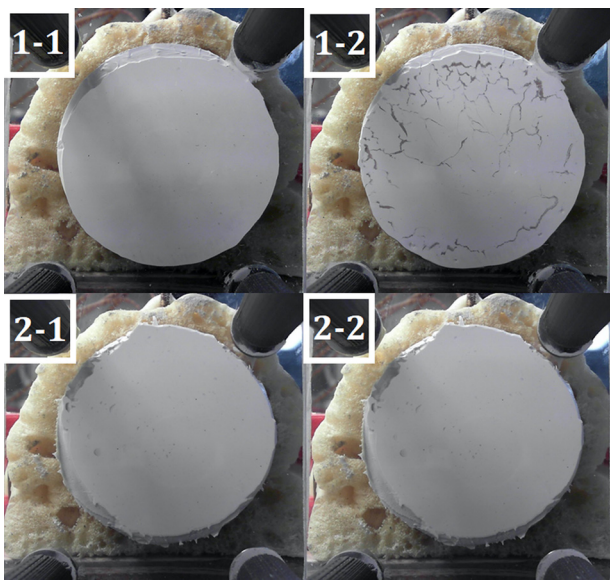

Fig. 6 Visual data of static testing: (1-1) prestatic test for paste 1, (1-2) poststatic test for paste 1, (2-1) prestatic test for paste 2, (2-2) poststatic test for paste 2

and nonsilicone paste matrix, which could make it more resilient to void formation and other thermal breakdown modes such as TIM dry-out. In terms of the observations from the static testing results, it is far too easy to simply say that paste 2 is superior to paste 1; however, the void formation of paste 1 from the static test would probably increase in severity with additional mechanical cycling, which would make it less than ideal for high temperature applications.

Cyclic Testing Results

Thermal Resistance Measurements. For the cyclic tests, each paste sample underwent a short 20 min equilibrium period in order to come to steady-state and was immediately followed by subsequent periods of mechanical cycling. As stated in the Materials and Methods section, the setup shown in Fig. 1 works effectively at monitoring the change in thermal resistance over time. In order to accurately depict this relative change, the thermal resistance measurement taken after each period of 100 cycles was compared as a relative difference from the initial resistance value, taken after the equilibrium period. This is simply calculated as $(R - R_i)/R_i$, where R is the measured resistance value, and R_i is the initial resistance measurement before cycling. Figure 7 represents the results of the cyclic testing for each loading condition and temperature performed on both thermal pastes. Each data point depicts a time-averaged resistance value from 100 s of temperature data following each period of cycling.

In the case of both pastes at 50 °C (top row of Fig. 7), the lower strain trials, 15% and 20%, displayed relatively miniscule deviation (<0.03) in thermal resistance even after 1000 cycles. A significant rise in resistance was not observed until the 30% strain/50 °C trial for paste 1, which had a relative change of over 0.158; regardless of the magnitude of this change in resistance, this test illustrates a dramatic thermomechanical failure of the polymer TIM, most likely as a result of void formation. This large relative rise in resistance is not seen in the same trial for paste 2. When the temperature is increased to 80 °C, paste 1 exhibited a similar, but lessened (when compared to the 30%/50 °C trial), increase in thermal resistance at a lower strain (20%), with the largest relative rise at 0.08. Again, for these trials, the change in resistance for paste 2 remains small. It is not until the strain is increased to 30% at 80 °C where paste 2 begins to have a significant increase in thermal resistance that is comparable to the relative change within the same trial for paste 1. A notable outlier can be seen in the 80 °C test for paste 1 at 15% strain, where the resistance initially decreases, then remains constant. We suspected that the small strain and elevated temperatures improved the thermal contact at the interface of the copper rods by removing small air pockets introduced during paste application. Basically, the actuator did not provide a large enough strain to instigate significant pump out behavior, which would be detrimental to the thermal performance of paste 1.

The results of these accelerated testing trials provide a glimpse into the multifaceted nature of thermal paste degradation. Obvious parallels can be drawn between paste viscosity, temperature at the interface, and their role in paste deterioration. In the case of both pastes 1 and 2, the role of temperature makes itself blatantly apparent; trials at 80 °C exhibited degradation behavior at a lower strain than the same trials at 50 °C. Paste 2, which resisted thermomechanical failure for nearly all the trials, observed its highest relative change in thermal resistance during the trial with the highest temperature and strain. An easy explanation for this occurrence can be found in their rheological properties; at the low strain rates exhibited by mechanical cycling ($< 1\,s^{-1}$), paste 2 resisted TIM pump-out and void formation simply because of its significantly higher viscosity than paste 2 at elevated temperatures. From the static testing, it can also be inferred that paste 2 is also more resistant to thermal breakdown in a stationary environment. Delineating how these variables affect thermal pastes during an accelerated mechanical cycling test can provide a means to accurately and quickly analyze their performance and determine their feasibility for a particular application.

Visualizing Cyclic Failure. A key component of this methodology stems from the ability to repeat the thermal resistance tests with the acrylic window apparatus and observe how thermomechanical cycling physically affects the paste specimens. Figure 8

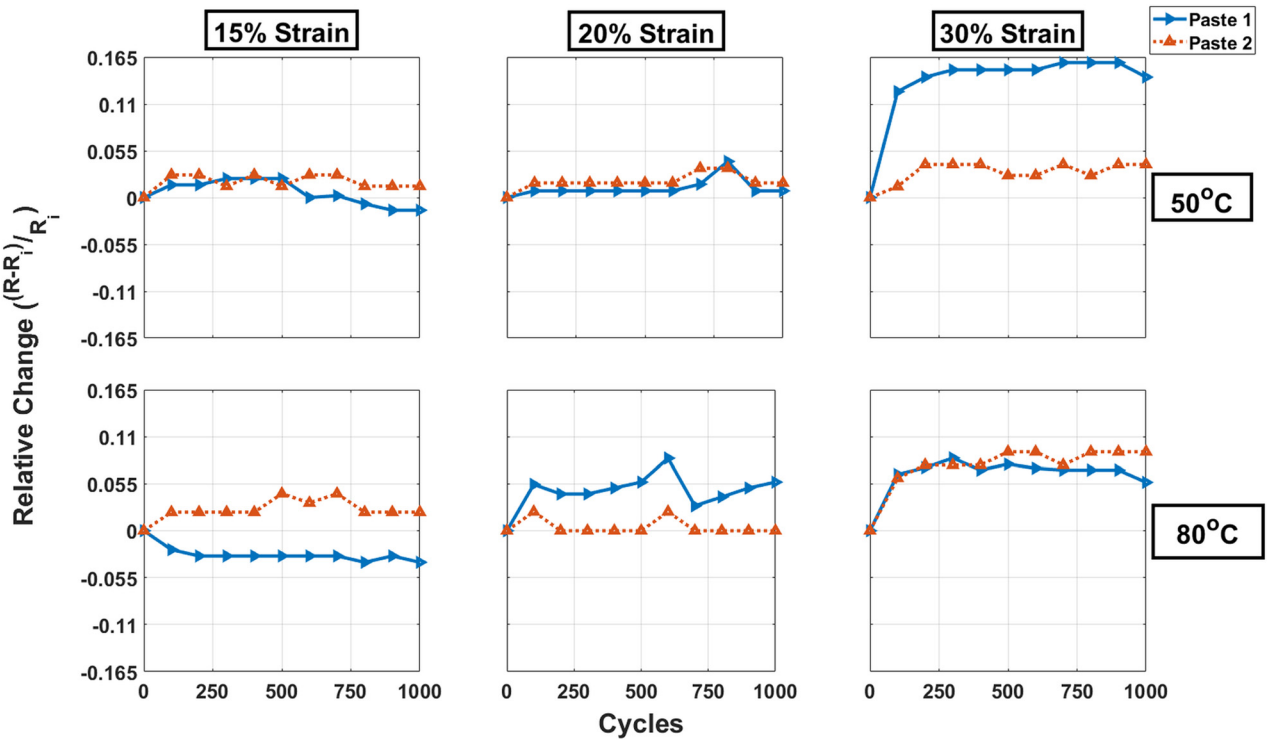

Fig. 7 Relative change in thermal resistance with respect to number of cycles and percent strain for 50 °C and 80 °C trials

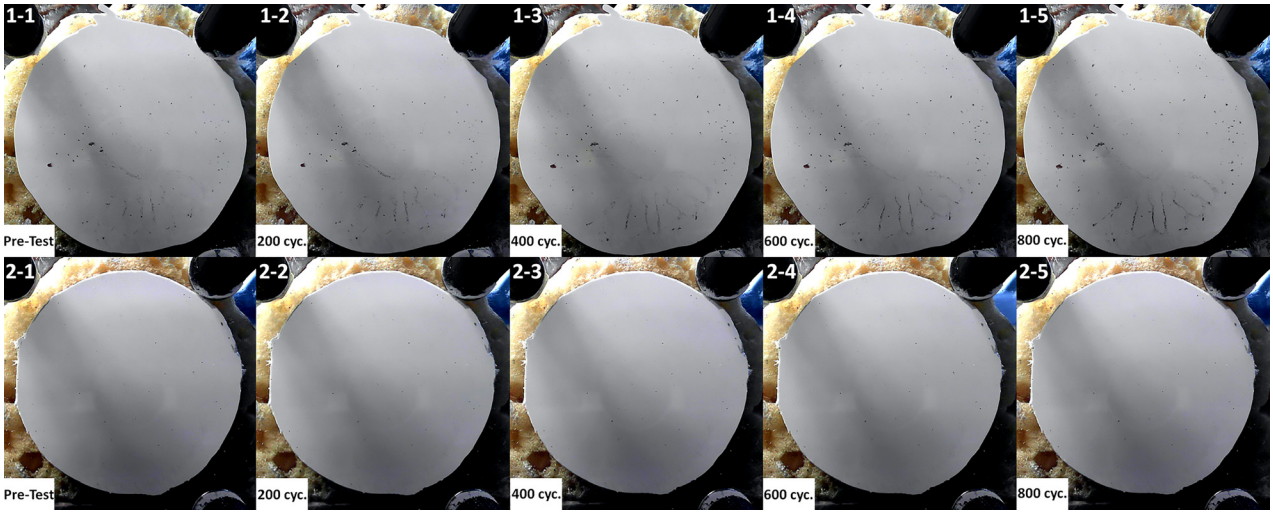

Fig. 8 Visual imagery of thermomechanical cyclic testing for both pastes at 80 °C and 15% strain: (1-1)–(1-5) paste 1 cyclic progression between the pretest and 800 cycles; (2-1)–(2-5) paste 2 cyclic progression between the pretest and 800 cycles

represents the 80 °C/15% strain trial performed in Fig. 7 for pastes 1 and 2. The progression begins with the image taken after the 20 min equilibrium (Pretest) and progresses with imagery taken after every 200 cycles. Even though none of the 15% strain trials caused a major relative change in thermal resistance, 15% strain was selected for the visual trial in order to determine if pump-out behavior occurred in a trial with minimal change in thermal resistance.

Similar to the appearance of the static tests, the pretest of paste 1 (1-1) displayed the onset of void formation, as indicated by the striations forming along the bottom half of the interface and smaller voids present around the edges. As paste 1 was continually cycled, the striations along the bottom not only became more pronounced, but the smaller voids, originally viewed during the pretest, became larger. Comparative measurements also indicate that the diameter of the circular interface expanded with the increased number of cycles, which further corroborates evidence for the occurrence of TIM pump-out. Unlike paste 1, with apparent evidence of TIM pump-out behavior, paste 2, observed no notable void formation throughout the entire trial. These images reinforce the thermal measurements discussed previously in illustrating how paste 2 resists thermomechanical degradation over subsequent cycles throughout the trial.

Conclusions

The work discussed herein introduced an accelerated method to analyze the thermomechanical breakdown of thermal pastes through a mechanical analog of thermal cycling. While normal thermal cycling tests used in industry can often take multiple weeks to determine thermal reliability, this mechanical cycling methodology can perform a reliability test within several hours. Regarding the two paste samples investigated, high strain with respect to the BLT during dynamic testing resulted in increased thermal resistance over the course of mechanical cycling. Thermal resistance also exhibited a dependency on local temperature, with higher temperatures resulting in accelerated paste degradation. Images taken during the static thermal test illustrated a vast disparity between the behaviors of the two paste types, specifically how the silicone oil paste specimen deteriorated to a higher degree than the nonsilicone oil paste when placed under constant loading and temperature. Visual imagery of the cyclic testing indicated that even at low strain rates, pump-out behavior still occurs and can be potentially be quantified with advanced image postprocessing.

Being able to visualize the interface in situ during a reliability test opens a new realm of possibilities for thermal paste failure analysis. Thermal/mechanical cycling tests provide a great deal of information regarding the dependency of paste reliability on variables such as material properties, number of cycles, strain, and temperature; however, the mode of failure can often not be easily observed as it occurs. Most of the analysis takes place immediately after testing, through techniques such as directly viewing the disassembled sample or scanning acoustic microscopy. While using acrylic or another clear material does not exactly mimic a copper–copper interface, its transparency provides a means to observe paste structure without disturbing the sample or utilizing complex experimental setups. In situ failure analysis provides a path to delineating failure modes, such as pump-out, and actively models their progression throughout the test. While the results of this visual study are largely qualitative, void formation, pump-out, and phase separation are all values that can be quantified and modeled through further image processing. Techniques such as the one described herein will aid in the development of more encompassing multiparameter models of thermal paste performance that not only describe the increase of thermal resistance (or junction temperature), but also how the physical structure of the paste changes during operating conditions. This type of testing can also be coupled with finite element analysis for predicting TIM degradation behaviors in traditional thermal cycling. Further developing methods such as this will reduce overall testing time in industry as well as create new ways to model how the structure of thermal pastes changes in application.

Acknowledgment

We would like to thank Ben Fleming, Jeff Knox, and John Carlton for their aid in the construction of the thermal conductivity tester apparatus. We are thankful to the University of Arkansas Engineering Research Center for providing the facilities that made this research possible. Any opinions, finding, and conclusions or recommendations expressed in this material are those of the author(s) and do not necessarily reflect the views of the National Science Foundation.

Funding Data

This effort was partially supported through the REU program under the POETS-ERC, under the National Science Foundation under Grant No. 2014-00555-04 (Funder ID: 10.13039/100000001).

Nomenclature

BLT = bond line thickness
d_{ij} = distance between thermocouples "i" and "j"

d_{is} = distance between thermocouple "i" and the surface of its respective rod
dT/dx = temperature gradient with respect to x-direction
k = thermal conductivity
R = thermal resistance
R_i = initial thermal resistance (0 cycles)
Q = total heat transfer
q_x = heat flux in x-direction
Q_{AVG} = average heat transfer across interface
Q_C = heat transfer through cooled rod
Q_H = heat transfer through heated rod
T_i = temperature at thermocouple "i"
TIM = thermal interface material
ΔT = change in temperature across interface

References

[1] Razeeb, K. M., Dalton, E., Cross, G. L. W., and Robinson, A. J., 2018, "Present and Future Thermal Interface Materials for Electronic Devices," Int. Mater. Rev., **63**(1), pp. 1–21.
[2] Hansson, J., Nilsson, T. M. J., Ye, L. L., and Liu, J., 2018, "Novel Nanostructured Thermal Interface Materials: A Review," Int. Mater. Rev., **63**(1), pp. 22–45.
[3] Due, J., and Robinson, A. J., 2013, "Reliability of Thermal Interface Materials: A Review," Appl. Therm. Eng., **50**(1), pp. 455–463.
[4] Roy, C. K., Bhavnani, S., Hamilton, M. C., Johnson, R. W., Nguyen, J. L., Knight, R. W., and Harris, D. K., 2015, "Investigation Into the Application of Low Melting Temperature Alloys as Wet Thermal Interface Materials," Int. J. Heat Mass Transfer, **85**, pp. 996–1002.
[5] Xu, J., and Fisher, T. S., 2006, "Enhancement of Thermal Interface Materials With Carbon Nanotube Arrays," Int. J. Heat Mass Transfer, **49**(9–10), pp. 1658–1666.
[6] Wunderle, B., Heilmann, J., May, D., Arnold, J., Hirscheider, J., Bauer, J., Schacht, R., Vogel, J., and Abo Ras, M., 2017, "Modelling and Characterisation of a Grease Pump-Out Test Stand and Its Use for Accelerated Stress Testing of Thermal Greases," 23rd International Workshop on Thermal Investigations of ICs and Systems (THERMINIC), Amsterdam, The Netherlands, Sept. 27–29, pp. 1–6.
[7] DeVoto, D., Paret, P., Mihalic, M., Narumanchi, S., Bar-Cohen, A., and Matin, K., 2014, "Thermal Performance and Reliability Characterization of Bonded Interface Materials (BIMs)," 14th Intersociety Conference on Thermal and Thermomechanical Phenomena in Electronic Systems, Orlando, FL, May 27–30, pp. 409–417.
[8] Warzoha, R. J., and Donovan, B. F., 2017, "High Resolution Steady-State Measurements of Thermal Contact Resistance Across Thermal Interface Material Junctions," Rev. Sci. Instrum., **88**(9), p. 094901.
[9] Sponagle, B., and Groulx, G., 2012, "Characterization of Thermal Interface Materials Using a Steady State Experimental Method," ASME Paper No. HT2012-58262.
[10] Székely, V., Vass-Várnai, A., and Kollár, E., 2010, "Re-Design and Validation of the 'STATIM' TIM Tester," 16th International Workshop on Thermal Investigations of ICs and Systems (THERMINIC), Barcelona, Spain, Oct. 6–8, pp. 1–4.
[11] Chen, C. I., Ni, C. Y., Chang, C. M., Liu, D. S., Pan, H. Y., and Yuan, T. D., 2008, "Thermal Characterization of Thermal Interface Materials," Exp. Tech., **32**(3), pp. 48–52.
[12] DeVoto, D., Major, J., Paret, P., Blackman, G. S., Wong, A., and Meth, J. S., 2017, "Degradation Characterization of Thermal Interface Greases," 16th IEEE Intersociety Conference on Thermal and Thermomechanical Phenomena in Electronic Systems (ITherm), Orlando, FL, May 30–June 2, pp. 394–399.
[13] Marbut, C. J., Montazeri, M., and Huitink, D. R., 2018, "Rapid Solder Interconnect Fatigue Life Test Methodology for Predicting Thermomechanical Reliability," IEEE Trans. Device Mater. Reliab., **18**(3), pp. 412–421.
[14] Gowda, A., Esler, D., Paisner, S. N., Tonapi, S., Nagarkar, K., and Srihari, K., 2005, "Reliability Testing of Silicone-Based Thermal Greases [IC Cooling Applications]," Semiconductor Thermal Measurement and Management IEEE Twenty First Annual IEEE Symposium, San Jose, CA, Mar. 15–17, pp. 64–71.
[15] Chia-Pin, C., Biju, C., Mello, K., and Kelley, K., 2001, "An Accelerated Reliability Test Method to Predict Thermal Grease Pump-Out in Flip-Chip Applications," Proceedings of the 51st Electronic Components and Technology Conference, Orlando, FL, May 29–June 1, pp. 91–97.
[16] Wunderle, B., May, D., Heilmann, J., Arnold, J., Hirscheider, J., Li, Y., Bauer, J., Schacht, R., and Ras, M. A., 2019, "Accelerated Pump Out Testing for Thermal Greases," 20th International Conference on Thermal, Mechanical and Multi-Physics Simulation and Experiments in Microelectronics and Microsystems, Hannover, Germany, March 24–27, p. 11.
[17] AboRas, M., May, D., Schacht, R., Winkler, T., Rzepka, S., Michel, B., and Wunderle, B., 2014, "Limitations and Accuracy of Steady State Technique for Thermal Characterization of Thermal Interface Materials and Substrates," Fourteenth Intersociety Conference on Thermal and Thermomechanical Phenomena in Electronic Systems (ITherm), Orlando, FL, May 27–30, pp. 1285–1293.